



Michigan Technological University
Create the Future Digital Commons @ Michigan Tech

Dissertations, Master's Theses and Master's
Reports - Open

Dissertations, Master's Theses and Master's
Reports

2014

DEVELOPMENT OF PRECIPITATION HARDENABLE AL-SC-ZR-HF QUATERNARY ALLOYS THROUGH THERMODYNAMIC MODELING, AND ROOM-TEMPERATURE AND ELEVATED TEMPERATURE HARDNESS

Matthew J. Wong
Michigan Technological University

Follow this and additional works at: <https://digitalcommons.mtu.edu/etds>


 Part of the [Materials Science and Engineering Commons](#)

Copyright 2014 Matthew J. Wong

Recommended Citation

Wong, Matthew J., "DEVELOPMENT OF PRECIPITATION HARDENABLE AL-SC-ZR-HF QUATERNARY ALLOYS THROUGH THERMODYNAMIC MODELING, AND ROOM-TEMPERATURE AND ELEVATED TEMPERATURE HARDNESS", Master's Thesis, Michigan Technological University, 2014.
<https://doi.org/10.37099/mtu.dc.etds/870>

Follow this and additional works at: <https://digitalcommons.mtu.edu/etds>

 Part of the [Materials Science and Engineering Commons](#)

DEVELOPMENT OF PRECIPITATION HARDENABLE AL-SC-ZR-HF
QUATERNARY ALLOYS THROUGH THERMODYNAMIC MODELING, AND
ROOM-TEMPERATURE AND ELEVATED TEMPERATURE HARDNESS

By
Matthew J. Wong

A THESIS

Submitted in partial fulfillment of the requirements for the degree of

MASTER OF SCIENCE

In Materials Science and Engineering

MICHIGAN TECHNOLOGICAL UNIVERSITY

2014

© 2014 Matthew J. Wong

This thesis has been approved in partial fulfillment of the requirements for the Degree of MASTER OF SCIENCE in Materials Science and Engineering.

Department of Materials Science and Engineering

Thesis Advisor: *Dr. Paul G. Sanders*

Committee Member: *Dr. Stephen L. Kampe*

Committee Member: *Dr. Scott A. Miers*

Department Chair: *Dr. Stephen L. Kampe*

Table of Contents

List of Figures	iv
List of Tables	vi
List of Abbreviations	vii
Preface.....	viii
Acknowledgements.....	ix
Abstract.....	x
1. Introduction.....	1
1.1 Strengthening Mechanisms in Aluminum Alloys.....	2
1.2 Selection Criteria for Precipitation Hardenable Aluminum Alloys.....	5
1.3 Building on Al-Sc-Zr Ternary Alloys.....	7
2. Hypotheses.....	10
3. Methods.....	11
3.1 Selection Criteria	11
3.2 Thermodynamic Modeling.....	13
3.3 Sample Preparation and Analytical Techniques	15
3.4 Aging.....	18
4. Results.....	19
4.1 Thermodynamic Modeling.....	19
4.2 Hardness and Conductivity.....	23
4.3 Microstructure.....	27
5. Discussion.....	30
6. Future Work	33
7. Conclusions.....	34
References.....	35
A. Appendix.....	37

List of Figures

Fig. 1-1	Particle strengthening diagram for spherical precipitates in a matrix.....	4
Fig. 1-2:	Al-rich portion of the Al-Sc binary phase diagram [6]	7
Fig. 1-3:	Al-rich portion of the Al-Zr phase diagram [10].....	8
Fig. 1-4:	Visualization of a coherent, core-shell Al_3Sc - Al_3Zr precipitate in α -Al matrix. The red and green spheres respresent the “ Al_3Sc ” and “ Al_3Zr ” structures, respectively, and the black spheres represent the α -Al matrix. This is not to scale for the relative lattice parameter mismatch.....	9
Fig. 3-1:	Simplex lattice design plot, 6th degree, showing the compositions to be analyzed. The sum is always 0.2 at%, where the balance is 99.8 at% Al.	13
Fig. 3-2:	As-cast arc-melted buttons.....	15
Fig. 3-3:	LECO MHT Series 200 Vickers microhardness tester.....	16
Fig. 3-4:	Vickers macroindenter with a motorized copper heating block for elevated-temperature hardness testing.	17
Fig. 3-5:	Multi-step, isochronal aging treatment showing the hold temperatures. Samples were water quenched after each temperature.....	18
Fig. 4-1:	Contour plot of total tri-aluminide precipitate fraction, Al_3M and Al_3Sc , at 650°C as a function of Sc, Zr, and Hf composition. Blue regions indicate low phase fraction, while green regions indicate high phase fractions....	19
Fig. 4-2:	Contour of total tri-aluminide precipitate fraction, Al_3M and Al_3Sc , at 400°C as a function of Sc, Zr, and Hf composition. Blue regions indicate low phase fraction, while green regions indicate high phase fractions....	20
Fig. 4-3:	The total change in precipitated phase fraction from 650°C to 400°C as a function of Sc, Zr, and Hf composition. Blue regions indicate low phase fraction, while green regions indicate high phase fractions.	21
Fig. 4-4:	Simplex design plot of the proposed quaternary Al-Sc-Zr-Hf alloy compositions.	22

Fig. 4-5:	Room-temperature microhardness profile of the quaternary alloys after each step of a multi-step, isochronal aging treatment.	23
Fig. 4-6:	Room temperature conductivity for a 3-hour multi-step, isochronal aging treatment up to 450°C, using an eddy-current conductivity meter.....	24
Fig. 4-7:	Elevated-temperature macrohardness profile for a 3-hour multi-step, isochronal aging treatment up to 450°C. This is the same thermal treatment as in Fig. 4-5 except the hardness was measured at elevated temperatures.....	25
Fig. 4-8:	Elevated-temperature macrohardness of various alloys	26
Fig. 4-9:	Room-temperature microhardness profile of the Al-Sc, Al-Zr, and Al-Hf binary alloys during a 3hr multi-step, isochronal heat-treatment.....	27
Fig. 4-10:	Bright-field TEM image of 0.125Sc-0.05Zr-0.025Hf showing a ripened precipitated, depleted zone, and unripened precipitates.	28
Fig. 4-11:	EDS scan from the α -Al matrix in 0.125Sc-0.05Zr-0.025Hf.	29
Fig. 4-12:	EDS scan of a precipitate in Al-0.125Sc-0.05Zr-0.025Hf, showing Sc, Zr, and the shoulder of an Hf peak on the peak from the Cu grid.	29
Fig. A-1:	Right to publish material from ASM for the Al-Sc Phase diagram from Fig. 1.2.	37
Fig. A-2:	Right to publish material from ASM for the Al-Zr Phase diagram from Fig. 1.3.	38

List of Tables

Table 3-1: Elemental Data for Select Elements in TCAL2 Database [1]	12
Table 3-2: Diffusion Data for Alloy Additions in Aluminum [1]	12
Table 4-1: Proposed Quaternary Compositions	21
Table 5-1: Diffusion Lengths in Aluminum after 3 hours	30
Table 5-2: Diffusion Lengths Through Aluminum After Each Heat Treatment Step	30

List of Abbreviations

T_M	melting temperature
fcc	face centered cubic
bcc	body centered cubic
hcp	hexagonal close packed
$L1_2$	ordered fcc lattice
DO_{24}	ordered hcp lattice
$\Delta\tau$	change in shear stress
Δc	change in composition
C	material constant (Eq 1)
G	shear modulus
ϵ	fractional change in lattice parameter (for Eq 1)
d	average grain size (Eq 2)
K_H	material constant (Eq 2)
$\Delta\sigma$	change in yield strength
b	Burgers vector
V_f	volume fraction
r	precipitate radius
γ'	Ni_3Al intermetallic
η	Ni_3Ti intermetallic
DOE	design of experiments
EDS	energy dispersive spectroscopy
TEM	transmission electron microscopy

Preface

Parts of this thesis will be submitted for publication in future, but has not been published previously. All of the following content is original to the author, and was not produced as a collaborative effort.

Acknowledgements

The following research would not have been possible without the guidance and patience of my advisor, Dr. Paul Sanders. I am grateful for him giving me the opportunity to be his student. I would like to thank the following people for their generous support and contributions to the work in this thesis:

Paul Fraley for assistance with arc-melting

Tom Wood for assistance with microhardness

Ruth Kramer for assistance with sample preparation

Owen Mills for assistance with microtome and TEM operation

Dan Sequin for assistance with TEM operation

And my fellow graduate students in the Solidification Theory and Practice group for their intellectual support: Kyle Deane, Marcel Kerkove, and Cameron McNamara.

I would also like to thank James Boileau and the Ford Motor Company for their generous financial support for this project, which allowed the work to be performed.

Abstract

Aluminum alloyed with small atomic fractions of Sc, Zr, and Hf has been shown to exhibit high temperature microstructural stability that may improve high temperature mechanical behavior. These quaternary alloys were designed using thermodynamic modeling to increase the volume fraction of precipitated tri-aluminide phases to improve thermal stability. When aged during a multi-step, isochronal heat treatment, two compositions showed a secondary room-temperature hardness peak up to 700 MPa at 450°C. Elevated temperature hardness profiles also indicated an increase in hardness from 200-300°C, attributed to the precipitation of Al₃Sc, however, no secondary hardness response was observed from the Al₃Zr or Al₃Hf phases in this alloy.

1. Introduction

Aluminum has been traditionally used in structures where high strength-to-weight ratios are required, including automotive and aerospace industries. The search for new alloying elements and combinations of strengthening effects is still actively investigated in aluminum. Increasingly, aluminum has begun to be utilized in systems at elevated temperatures, something generally avoided because of its drastic reduction in mechanical strength near $0.54 \cdot T_M$ ($\sim 230^\circ\text{C}$) [1]. However, like the widely used high-temperature Ni-based alloys, Al alloys share the same face-centered cubic (fcc) crystal structure. This is beneficial for high-temperature creep resistance as it has closer-packed atomic planes than that of more open structures like body-centered cubic (bcc) materials, which have a greater number of slip systems. Additionally, the natural oxidation resistance of Al is beneficial for high-temperature applications as it forms a protective oxide layer on its surface [2]. However, aluminum's challenge with thermal stability is its inability to form high volume fractions of strengthening phases like those used Ni-based alloy. By creatively using different alloying strategies and strengthening mechanisms, it may be possible to produce enhanced high-temperature mechanical properties in aluminum, thus taking advantage of aluminum's sought-after high strength-to-weight performance.

1.1 Strengthening Mechanisms in Aluminum Alloys

Aluminum can be strengthened through several different mechanisms that restrict deformation by dislocation motion, including strain-hardening, solid-solution hardening, grain size hardening, and precipitate hardening. Traditionally, high production volume aluminum alloys use these mechanisms individually or in combination with another [1].

Strain-hardening increases the strength of a ductile material by producing high dislocation density through deformation. As dislocation density increases, more shear stress is needed for subsequent dislocations to be generated and displaced through the material. In solid-solution hardened alloys, solute atoms strengthen the matrix due to their size and modulus differences. This causes an increase in the force needed for dislocations to pass through the strained lattice. The increase in yield strength, $\Delta\sigma_{ys}$, is proportional to the concentration of solute atoms, and follows a 4/3 power law, based upon the misfit of the lattice parameter. This can be seen in Eq. 1,

$$\Delta\tau/\Delta c = C \cdot G \cdot \varepsilon^{4/3} \quad (\text{Eq. 1})$$

where ε is the fractional lattice parameter change, c is the concentration, E is the elastic modulus, and C is a constant [1].

Grain size hardening works on the basis that grain boundaries act as a barrier to dislocation movement. As the grain size decreases, the number of these barriers present to impede dislocations also increases. The yield strength increase is inversely proportional to the grain size, as governed by the Hall-Petch relationship. This relationship shows the increase in yield strength is proportional to the inverse square root of the average grain size, d , shown in Eq. 2,

$$\Delta\tau = K_H d^{-1/2} \quad (\text{Eq. 2})$$

where K_H is a constant [1].

Precipitation hardening is produced when a material has a fine distribution of particles within a matrix. For a dislocation to pass a particle, it must either bow around or cut through the particle; this is dependent on the size of the particles. The former was first suggested by Orowan, where the energy required for a dislocation to bow around a particle is inversely proportional to the particle spacing. Thus, for a given volume fraction of a precipitated phase, as the particles decrease in size, the number density increases, thus decreasing the inter-particle spacing and increasing the energy needed to bow around the particles. In the latter, there is an energy increase proportional to the square root of the particle size [1] related to the increase in particle surface area after it has been cut as a dislocation. Small particles are generally soft to dislocation motion, and will shear easily, but as the particle size increases, it becomes hard to dislocation motion. During late stages of precipitation, larger precipitates continue to grow at the expense of the smaller ones to reduce surface energy. This overaging is due to Ostwald ripening, which further decreases the overall strength of the alloy. The quantification of precipitation hardening is shown in Eq. 3, where the shear stress needed to bow the dislocation around the particle, τ , as suggested by Orowan, is

$$\tau = 2 \cdot G \cdot b \cdot (V_f / \pi)^{1/2} \cdot r^{-1} \quad (\text{Eq. 3})$$

where G is the shear modulus, b is the Burgers vector, V_f is the volume fraction of precipitates, and r is the precipitate radius. The strength increases with increasing volume fraction and decreasing precipitate size [1]. If the dislocation is able to cut through the particle, the governing equation is linearly dependent on particle size, shown in Eq. 4,

$$\tau = \pi \cdot r \cdot \gamma \cdot (b \cdot L)^{-1} \quad (\text{Eq. 4})$$

where r is the precipitate radius, γ is the surface energy, b is the Burgers vector, and L is the spacing between particles. These two equations can be plotted on the same graph to show how the transition between particle cutting and bowing is dependent on particle size (Fig. 1-1). This shows that there is a critical radius where the maximum precipitation strengthening can be achieved.

However, alloys for high-temperature applications may require a combination of strengthening mechanisms, as more modes of deformation are activated. Plastic deformation through dislocation creep occurs as dislocation motion becomes easier due to higher thermal energy at higher temperatures, which assists in circumventing barriers. As atoms increase their energy with increasing temperature, their vibrations can lead to vacancy mediated dislocation climb. Also, as grains begin to recrystallize, dislocations can be annihilated. It is important, therefore, that dislocation motion must continue to be resisted at elevated temperatures. In general, precipitation hardening is considered one of the more effective mechanisms for strengthening metals [1]. Therefore, to reduce the loss in strength when exposed to high-temperatures, stabilizing the precipitate morphology is critical.

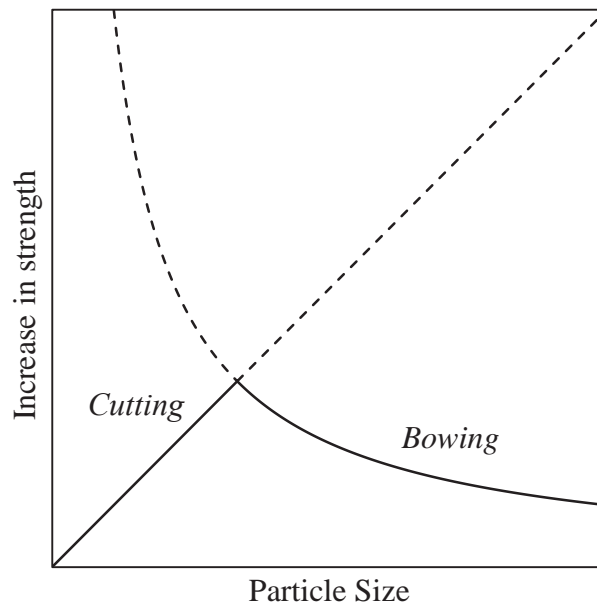


Fig. 1-1 Particle strengthening diagram for spherical precipitates in a matrix.

1.2 Selection Criteria for Precipitation Hardenable Aluminum Alloys

Not all alloying additions to Al will result in effective precipitation hardening. Knipling, et al. proposed a set of criteria for selecting elements that would be effective additions for producing a precipitation hardenable alloys [2]. This includes the ability to form coherent intermetallic precipitates, low solute solubility in Al, a shallow solvus curve, and low diffusivity in Al.

Intermetallics have been used in analogous systems, such as Ni, to increase creep resistance at high temperatures. Most Ni-based superalloys use a γ' (Ni_3Al) precipitate, which has an $L1_2$ structure and is coherent with the fcc matrix. Knipling extends this analog to aluminum by proposing tri-aluminide intermetallics, using the form Al_3M , where “M” is an element within the transition metals or lanthanide or actinide series. However, most tri-aluminide intermetallics do not have $L1_2$ structures, but similar hexagonal close-packed (hcp) or tetragonal structures. Though not completely coherent due to large stacking sequences, many of their structures have similar stacking sequences to those in fcc lattices. This can be manipulated into metastable $L1_2$ phases, which are found in a number of tri-aluminides, such as those found in Group IV and V transition metals [2].

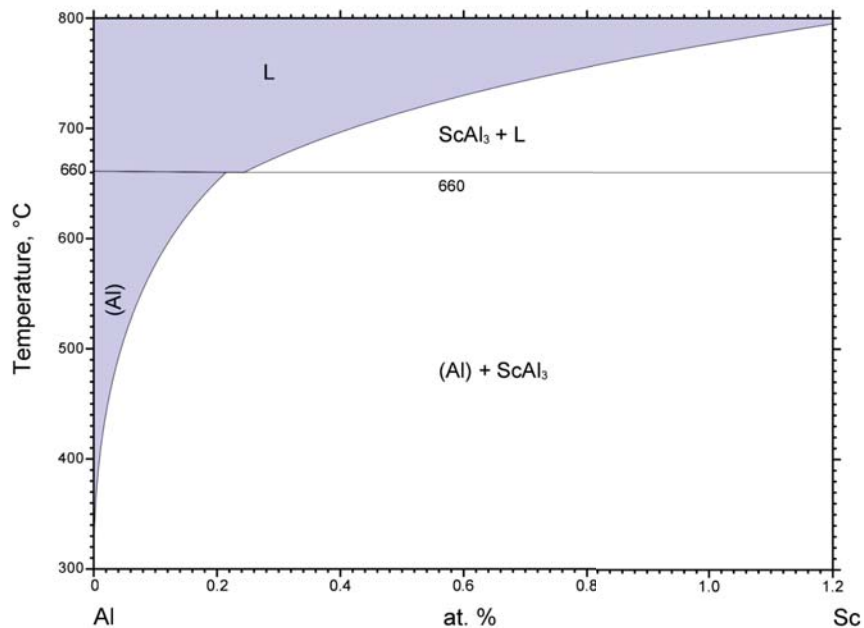
For precipitation hardenable alloys, it is advantageous for there to be a significant change in solubility between the max solubility and that near the aging temperature. This allows the most solute to come out of solution to form ordered intermetallics. Many of the transition metals, most notably those in Groups III, IV, and V, have low solubilities at all temperatures (<0.5 at%). Additionally, for the Al_3M precipitate to form from solid-solution, it must be the terminal phase with α -Al (the most Al-rich phase) [2].

One other aspect that is advantageous for creep resistant materials is thermal stability of the strengthening phase. This can be characterized kinetically by the relative diffusion coefficients of the alloying elements, or the diffusivities in α -Al. Many of the Group III, IV, and V elements are quite slow diffusers compared to those found in higher weight transition elements. However, it must be noted that those with much lower diffusion rates

(i.e. Ti) can lead to unreasonable aging times, as it would take too long for those elements to reach a nominal diffusion length required to coalesce into a precipitate. High-temperature stability of precipitated phases also relies on coarsening resistance. This can be achieved by reducing the driving force for Ostwald ripening, or dissolution into the matrix. Low lattice-mismatch can stabilize the particle coherency by decreasing the surface energy between the particle and the matrix [2].

1.3 Building on Al-Sc-Zr Ternary Alloys

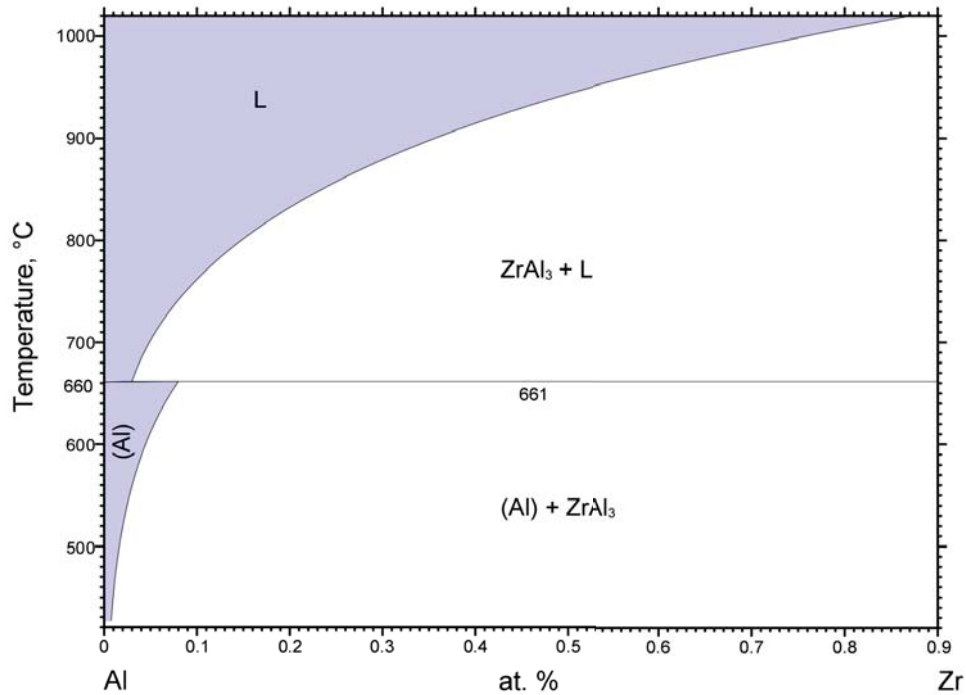
Scandium is gaining much attention as a potential alloying addition to Al since the granting of a patent in the early 1970s [3]. The addition of Sc significantly improves the strength of Al, even though it has relatively low solubility. It also augments many strengthening mechanisms, as it refines grain size, retards recrystallization, and precipitates into a coherent $L1_2$ Al_3Sc phase [4]. However, Sc can remain in solution well beyond its maximum equilibrium solubility, especially when high (10^7 K/s) cooling rates are used [5]. A low solubility of less than 0.01 at% below $400^\circ C$ enables most solute to form precipitates increasing the volume fraction. This can be seen in the Al-rich portion of the phase diagram in Fig. 1.1 [6]. The Al_3Sc precipitates also benefit from good thermal stability, where they remain stable up to $300^\circ C$, before Ostwald ripening leads to decreases in strength [7,8].



© ASM International 2012. Diagram No. 104019

Fig. 1-2: Al-rich portion of the Al-Sc binary phase diagram [6]

Other elements have also been added to Al-Sc alloys, with many studies showing synergistic effects from Zr additions [5,7-9]. It benefits from having very low solubility in Al, as shown in the Al-rich portion of the phase diagram, in Fig. 1.2 [10]. However, it is not advantageous to use alone as a primary precipitation strengthener, as Al_3Zr forms a peritectic with $\alpha\text{-Al}$ which causes segregation during solidification. Homogenization is also not possible as stable Al_3Zr precipitates are D0_{23} , which are incoherent with the fcc $\alpha\text{-Al}$.



© ASM International 2006. Diagram No. 1600336.

Fig. 1-3: Al-rich portion of the Al-Zr phase diagram [10]

When combined into ternary compositions, multi-step isochronal heat treatments yield hardness profiles with attributes of both binaries. A study by Knipling, et al. with Al-0.1at%Sc, Al-0.1at%Zr, and Al-0.1at%Sc-0.1at%Zr illustrates this trend. The initial hardness increase of the ternary occurs at about the same time as the Al-Sc binary profile, which would indicate the nucleation of Al_3Sc precipitates. However, with the addition of Zr, the hardening effect is continued up to 400°C. This is due to the ability for Zr to diffuse

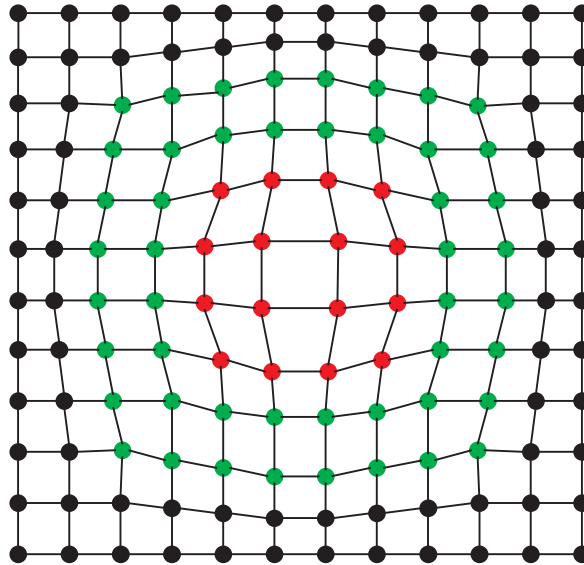


Fig. 1-4: Visualization of a coherent, core-shell $\text{Al}_3\text{Sc}-\text{Al}_3\text{Zr}$ precipitate in $\alpha\text{-Al}$ matrix. The red and green spheres represent the “ Al_3Sc ” and “ Al_3Zr ” structures, respectively, and the black spheres represent the $\alpha\text{-Al}$ matrix. This is not to scale for the relative lattice parameter mismatch.

to the Al_3Sc cores, creating a “core-shell” microstructure in which the precipitate maintains the coherent $L1_2$ structure [7,8]. This can be visualized as a nano-spherical particle, like that shown in Fig. 1.4.

2. Hypotheses

Al-Sc-Zr ternary alloys have already been studied by Knipling, et al [2,7-9]. However, the high temperature strengths of these alloys are limited by the rapid precipitate coarsening kinetics above 400°C. The goal of this research is to produce a quaternary alloy system that has enhanced coarsening resistance as compared to Al-Sc-Zr ternary alloys at temperatures above 400°C.

1. If Hf is added to the Al-Sc-Zr system, then a second shell will form around the Al₃Sc-core/Al₃Zr-shell precipitate structure in a multi-step, isochronal heat treatment because Hf will diffuse at higher temperatures forming a second shell around the Sc and Zr which have already precipitated out.
2. If Hf is added to a low-alloy Al-Sc-Zr ternary system, then the new quaternary system will retain the strength of the ternary system to higher temperatures because the diffusion kinetics of Hf are slower than Sc and Zr, and the lattice parameter of Al₃Hf is closer that of α -Al, which will produce a precipitate with greater coarsening resistance.

3. Methods

3.1 Selection Criteria

An abbreviated list of elements of interest can be found in Table 3.1, which are the elements that are present in the Thermo-Calc¹ database TCAL2 and produce the Al₃X precipitate phase. Many of these elements, however, do not fulfill the requirements set by Knipling, such as having a stable or metastable L1₂ structure, having a shallow solvus curve, or having low diffusivity in Al. Of those elements in Table 3.1, Hf and Ti show the most promise for precipitation hardening ability. However, Ti has been shown to remain in solution after extended aging times, and thus will not be tested [12]. This leaves Hf, which has not been investigated in quaternary systems [13]. It should also be noted that there are uncertainties in the quality of the phase diagrams in dilute Al-Sc-Zr-Hf systems, where predicted maximum solubilities are higher than those observed in experimental systems.

Table 3.2 shows a comparison of diffusion data for Sc, Zr, and Hf. With these rates, Sc will begin to diffuse at lower temperatures than Zr and Hf. As the temperature increases, Zr should be the next to precipitate out, and Hf should be the last.

¹ Thermo-Calc is a registered trademark of Thermo-Calc Software AB, Norro Stationsgatan, Sweden

Table 3-1: Elemental Data for Select Elements in TCAL2 Database [1]

Partial List of Elements	Al ₃ X	Al ₃ X in Eq with α -Al	Crystal Structure	Mismatch with Al (%)	Diffusivity at 400°C (m ² s ⁻¹)
Co	√	No	Orthorhombic	--	1.76x10 ⁻¹⁵
Hf	√	√	D0 ₂₃	--	2.11x10 ⁻²¹
			L1 ₂	-0.04	
La	√	No	Hexagonal	--	2.43x10 ⁻¹⁹
Ni	√	√	Orthorhombic	--	2.05x10 ⁻¹⁵
Sc	√	√	L1 ₂	1.32	1.98x10 ⁻¹⁷
Ti	√	√	D0 ₂₂	--	7.39x10 ⁻²²
			L1 ₂	-2.04	
V	√	No	D0 ₂₂	--	4.85x10 ⁻²⁴
			L1 ₂	-4.44	
Zr	√	√	D0 ₂₃	--	1.20x10 ⁻²⁰
			L1 ₂	4.08	

^aBased on elements found in the Thermo-Calc TCAL2 database

Table 3-2: Diffusion Data for Alloy Additions in Aluminum [1]

	Pre-Exponential, D_0 m ² ·s ⁻¹	Activation Enthalpy, Q kJ·mol ⁻¹	D at 200°C	D at 300°C m ² ·s ⁻¹	D at 400°C
Sc	5.31×10 ⁻⁴	173	4.17×10 ⁻²³	9.00×10 ⁻²⁰	1.98×10 ⁻¹⁷
Zr	7.28×10 ⁻²	242	1.37×10 ⁻²⁸	6.33×10 ⁻²⁴	1.20×10 ⁻²⁰
Hf	1.07×10 ⁻²	241	2.60×10 ⁻²⁹	1.15×10 ⁻³⁴	2.11×10 ⁻²¹

3.2 Thermodynamic Modeling

Ternary mixture designed experiments were used to analyze three-way interactions of the alloying additions of Al_3X precipitates in the α -Al matrix. This method allows graphical representation of alloy behavior, analogous to a ternary isothermal section of the phase diagram. Minitab contains three different experimental mixture designs, including simplex centroid, simplex lattice, and extreme vertices. In this designed experiment, only the simplex lattice design was utilized for its ability to analyze lattice points across an entire composition range, including axial points. In this specific design of experiments (DOE), a set atomic fraction of 0.2 at% was used as the total fraction of the solute additions, leaving the fraction of Al at 99.8 at%. The data points used in each experiment can be seen in Fig. 3.1.

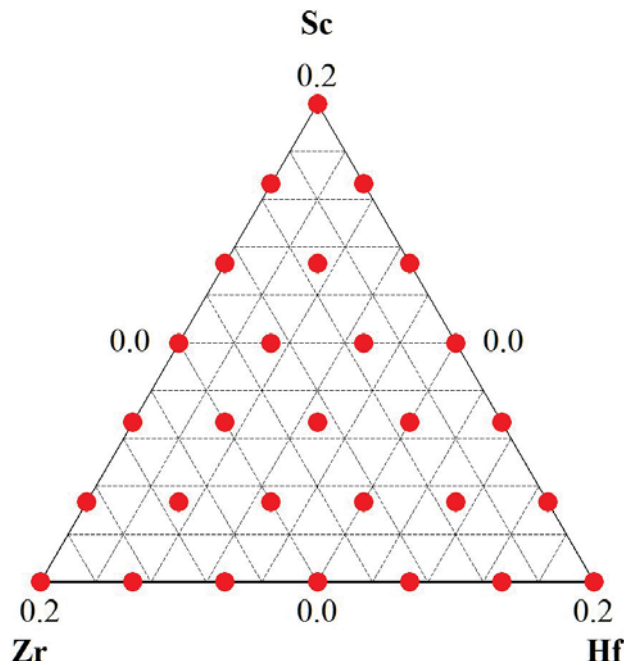


Fig. 3-1: Simplex lattice design plot, 6th degree, showing the compositions to be analyzed. The sum is always 0.2 at%, where the balance is 99.8 at% Al.

The metrics used to quantify the effects of the 3rd alloy addition to the ternary Al-Sc-Zr system included the total fraction of all precipitated phases, total fraction of specific phases, and the difference in the precipitated phases compared to the base Al-Sc-Zr alloys.

The Thermo-Calc software package with the TCAL2 database were used to predict the relative fractions of several phases. It is based on a minimization of Gibbs free energy curves for varying compositions, and calculates the equilibrium phases present for the given parameters. For this experiment, the most important phases of interest were those that had an FCC-L1₂ type structure, such as the stable Al₃Sc and metastable Al₃Zr and Al₃Hf. In Thermo-Calc, these phases were represented as Al₃Sc, and Al₃M, where “M” is the placeholder for varying metals. The two temperatures of interest were 400°C and 650°C. Homogenizing of the alloy at 650°C, which is close to the melting temperature (660°C for Al), puts the maximum quantity of solute in solution (minimum volume fraction of precipitates). A temperature of 400°C was used as an upper bound of the “aging” range in which precipitation occurs.

3.3 *Sample Preparation and Analytical Techniques*

Each alloy was prepared by arc-melting into buttons in a purified Ar atmosphere. The sample chamber was pumped down three times to a pressure of ___ atmospheres, and backfilled with Ar gas. Each button was flipped a minimum of three times to ensure a homogenous composition. Between each melt, a Ti-getter was heated to pull any outgasses from the chamber. The holder was a solid, water-chilled block of Cu. Pure Al (99.99%) was used to dilute the Sc and Zr master alloy additions (1.2 wt% and 10 wt%, respectively), and Hf (99.8% Hf with primarily Zr impurity, pellets). Each arc-melted button was approximately 20 grams, shown in Fig. 3.3, and cleaned using a 5% NaOH solution in water for 30 minutes, prior to planing parallel surfaces with a 120 grit wheel. The buttons were mechanically polished to remove any scratches that might interfere with measuring Vickers diamond indents.



Fig. 3-2: As-cast arc-melted buttons

Vickers microhardness measurements were taken at room-temperature on as-polished sample surfaces using a LECO MHT Series 200 (Fig. 3.4). A 10 g load and a dwell time of 10 s were used on each sample with a minimum of 15 measurements per sample for each temperature. The measurements were taken on the metallographically polished, parallel surface. Uncertainties shown are in two standard errors from the mean.



Fig. 3-3: LECO MHT Series 200 Vickers microhardness tester

For elevated-temperature hardness, a Vickers macroindenter was equipped with a heated, mechanically operated stage shown in (Fig. 3.5). A 1 kg load and a 5 s dwell time were used on each sample with a minimum of 3 measurements per sample at each temperature. A 99.99% Al test block was used to set a reference hardness at each temperature step. The samples were then repolished to remove any oxide before being heated to the testing temperature in air for a minimum of 15 minutes to reach equilibrium before the first indentation was made. Uncertainties shown are two standard errors from the mean.

Conductivity measurements were performed after each heat treatment step using an eddy current meter (Fischer Sigmascope SMP 10). A minimum of 5 measurements were taken for each sample at each temperature, on the polished surface, prior to hardness testing. Uncertainties shown are two standard error from the mean.



Fig. 3-4: Vickers macroindenter with a motorized copper heating block for elevated-temperature hardness testing.

For TEM analysis, arc-melted buttons were filed down to a powder. The powder was encased in a quartz tube under vacuum. These samples were heat treated using the same multi-step, isochronal procedure as done for hardness measurements. The powder was then encapsulated in epoxy and sliced into thin sections using ultramicrotomy. A JEOL JEM-2010 TEM was used to both image precipitate morphology and measure the composition of the precipitates using the EDS system. A 200kV accelerating voltage was used for both imaging and qualitative EDS analysis. A 60 s live time was used for all EDS scans, with roughly 10-20% dead time.

Grain size measurements were made on polished surfaces, etched with Keller's reagent to reveal the grain boundaries, according to ASTM E-112 standards.

3.4 Aging

Two aging conditions were examined in this study. The first was a multi-step, isochronal aging treatment used by Knipling, shown in Fig. 3-5. For room temperature hardness, each sample was held at temperature for 3 hours, after which they were removed and water quenched, and repolished before measuring the conductivity and hardness. For elevated hardness tests, the samples were held for 3 hours, removed from the furnace, and then reheated to same temperature in the hot-hardness tester. The alloys that were aged according to this procedure included 4 quaternary alloys, and three binary alloys (Al-0.1at%Sc, Al-0.1at%Zr, and Al-0.1at%Hf).

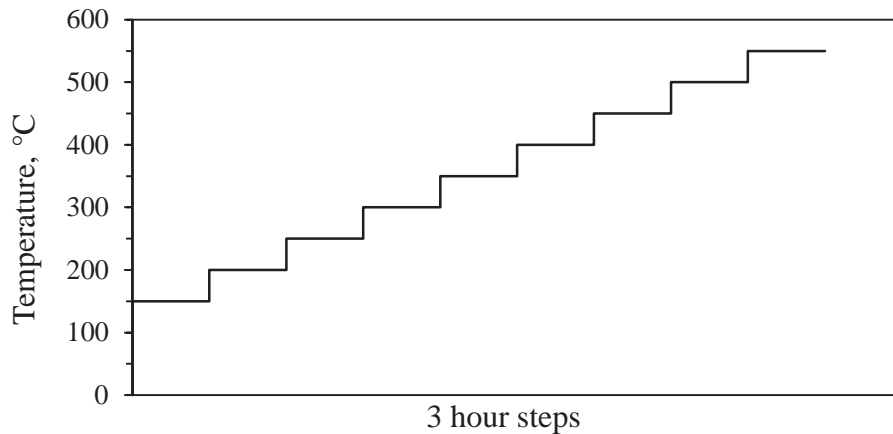


Fig. 3-5: Multi-step, isochronal aging treatment showing the hold temperatures. Samples were water quenched after each temperature.

The second aging treatment was a peak-aging heat treatment to form a “core-shell-shell” microstructure. This was done using a three-step heat-treatment, shown in Table 3-1, and was done on the 4 quaternary compositions, but were different heats than the multi-step, isochronal aging treatment. These alloys were measured using elevated-temperature hardness and compared to two commercially available alloys, A356, and a piston alloy provided by the Ford Motor Company, the compositions of which are shown in Table 3-2. Additionally, one composition was then re-tested to simulate an overaging-type condition to compare directly with the Ford piston, which was received under a T-7 condition.

4. Results

4.1 Thermodynamic Modeling

Figures 4.1-4.3 show contour plots from the mixture DOE composed of combinations of 0.2 at% Sc, Zr, and Hf in 99.8 at% Al. Figure 4.1 shows the interaction between the three alloying elements and the formation of the tri-aluminide precipitates at 650°C. This indicates that high Zr levels can lead to primary precipitation near the melting point of Al, which is not beneficial for creating a homogenous as-cast microstructure or for strengthening.

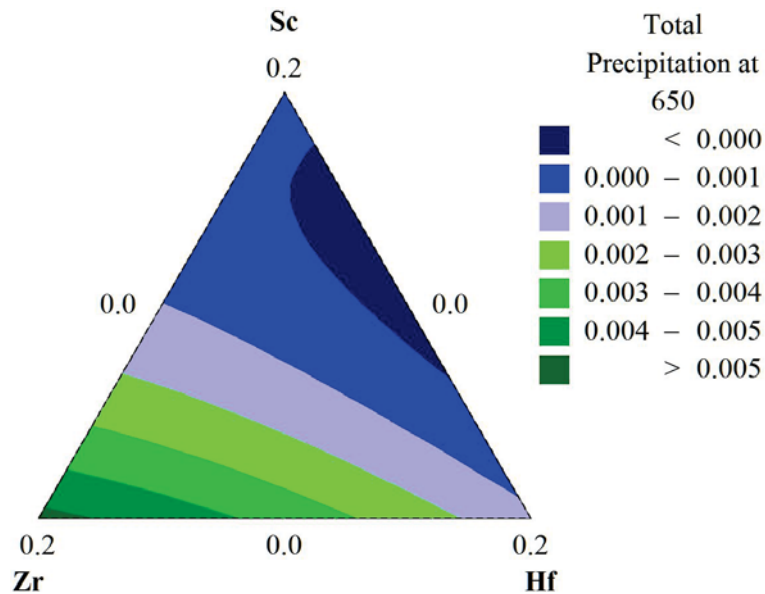


Fig. 4-1: Contour plot of total tri-aluminide precipitate fraction, Al_3M and Al_3Sc , at 650°C as a function of Sc, Zr, and Hf composition. Blue regions indicate low phase fraction, while green regions indicate high phase fractions.

Figure 4.2 shows the precipitation of the tri-aluminide phases at 400°C, or the upper bound for an aging-temperature. This indicates that higher levels of either Sc, Zr, or Hf can lead to higher precipitation fractions, while along the binary Sc-Hf is a local minima for total precipitate fraction. Note that the range of this in Fig. 4-2 is less than in Fig. 4-1.

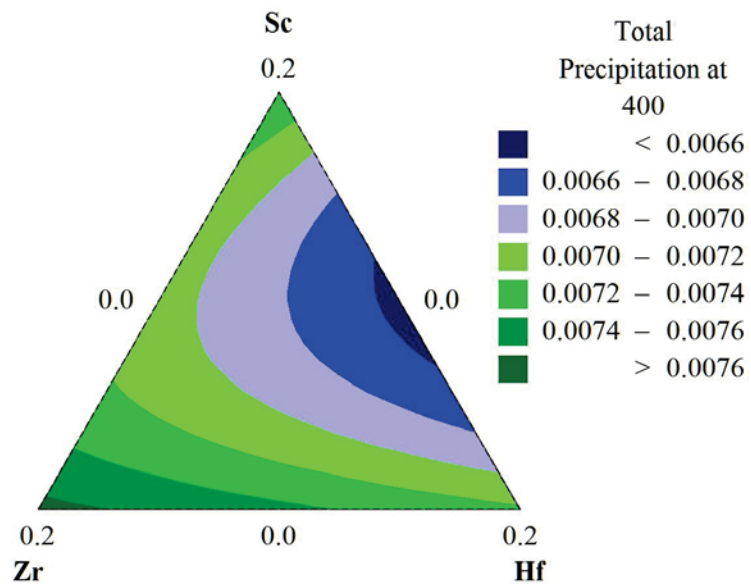


Fig. 4-2: Contour of total tri-aluminide precipitate fraction, Al₃M and Al₃Sc, at 400°C as a function of Sc, Zr, and Hf composition. Blue regions indicate low phase fraction, while green regions indicate high phase fractions.

By looking at the difference of these two contour plots, the effects on total precipitation from the as-cast structure can be seen; this is shown in Fig. 4.3. High levels of Sc show the most effect on the change in overall precipitation from 650°C to 400°C. However, Hf also shows an effect, where the contours show slight curvature to the Hf rich corner.

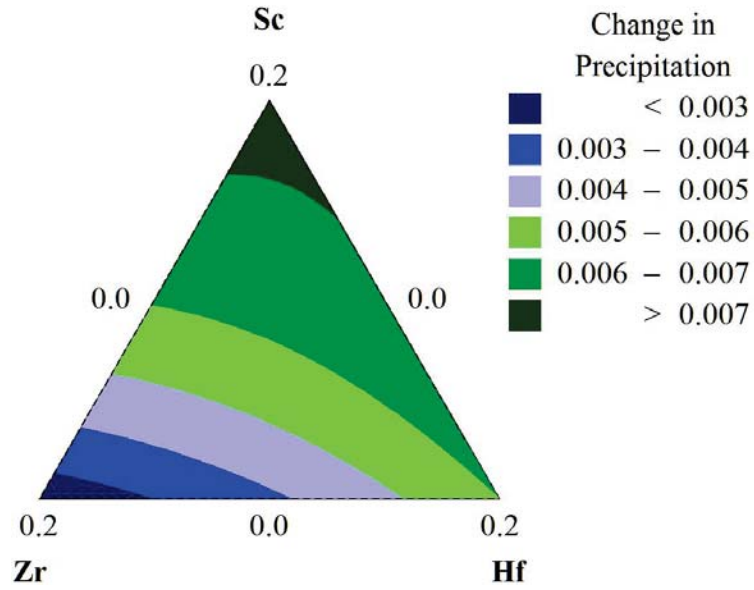


Fig. 4-3: The total change in precipitated phase fraction from 650°C to 400°C as a function of Sc, Zr, and Hf composition. Blue regions indicate low phase fraction, while green regions indicate high phase fractions.

Though no global quaternary maxima is seen in this last plot, it does show an area of where the change in slope is decreasing towards the Sc rich corner. Given uncertainty in the database, it was decided to explore this region experimentally via aging treatments and hardness measurements, where four compositions near the Sc-rich corner were made via arc-melting. This composition set can be seen in Table 4.1 and Fig. 4.4.

Table 4-1: Proposed Quaternary Compositions

Sample	Sc	Zr	Hf	Al
	Atomic Pct.			
1	0.150	0.025	0.025	99.8
2	0.125	0.050	0.025	99.8
3	0.125	0.025	0.050	99.8
4	0.100	0.050	0.050	99.8

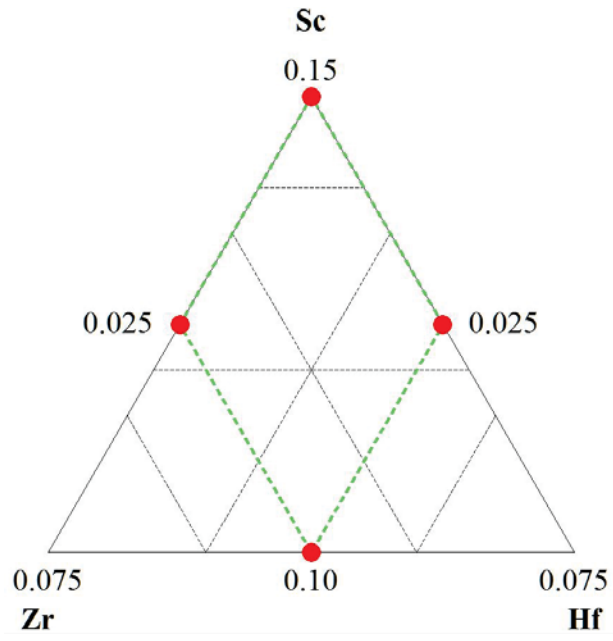


Fig. 4-4: Simplex design plot of the proposed quaternary Al-Sc-Zr-Hf alloy compositions.

4.2 Hardness and Conductivity

Room-temperature microhardness results after a 3-hour multi-step, isochronal heat-treatment are shown in Fig. 4.5. The four compositions show large increase in hardness beginning after aging at 250°C, with a peak hardness of 680-800 MPa, between 300°C and 350°C. A gradual decrease begins at 400°C. While the 0.15Sc-0.025Zr-0.025Hf and 0.125Sc-0.25Zr-0.05Hf (low Zr concentration) both monotonically decrease above 400°C, the 0.125Sc-0.05Zr-0.025Hf and the 0.1-Sc-0.05Zr-0.05Hf (high Zr concentration) compositions show a slight second peak at 450°C, between 650-700 MPa. Conductivity, shown in Fig. 4.7, also increases from 29-30 $\text{Ms}\cdot\text{m}^{-1}$ at 250°C, peaking to 33-34 $\text{Ms}\cdot\text{m}^{-1}$ at 450°C, indicating the maximum, total precipitation occurring up to 450°C.

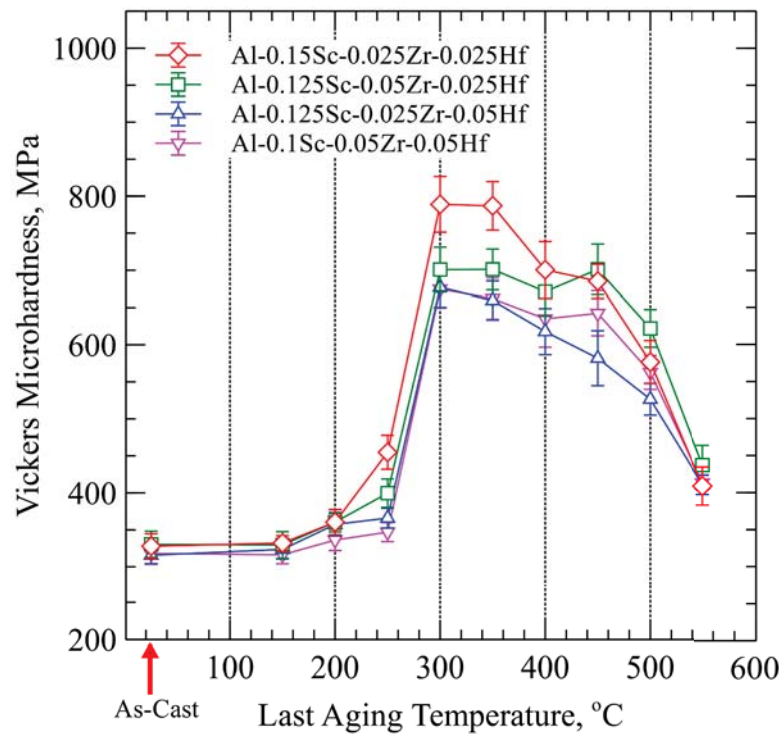


Fig. 4-5: Room-temperature microhardness profile of the quaternary alloys after each step of a multi-step, isochronal aging treatment.

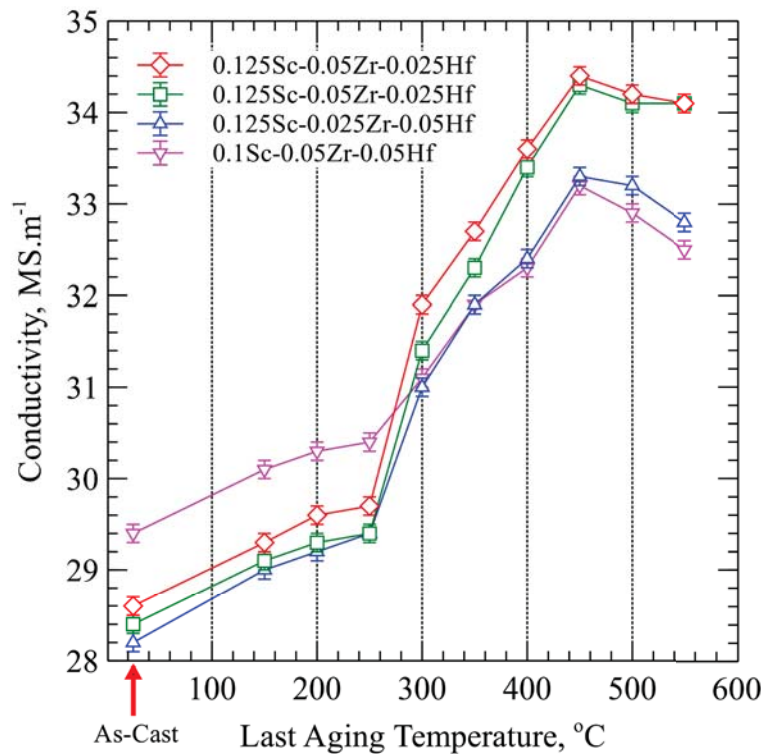


Fig. 4-6: Room temperature conductivity for a 3-hour multi-step, isochronal aging treatment up to 450°C, using an eddy-current conductivity meter.

A profile comparing elevated-temperature macrohardness is shown in Fig. 4.6. A 99.99% pure Al block was used to set a reference curve to compare the hardness with the four compositions. The Al block has a negative, linear correlation between temperature and hardness, starting at 166 MPa at room-temperature, decreasing to 29 MPa by 400°C. The four alloy compositions all have a sharp decrease in hardness at 150°C, however, between 200°C and 300°C, the hardness shows a plateau (except for the Al-0.1Sc-0.05Zr-0.05Hf), and steady decrease in hardness above 300°C.

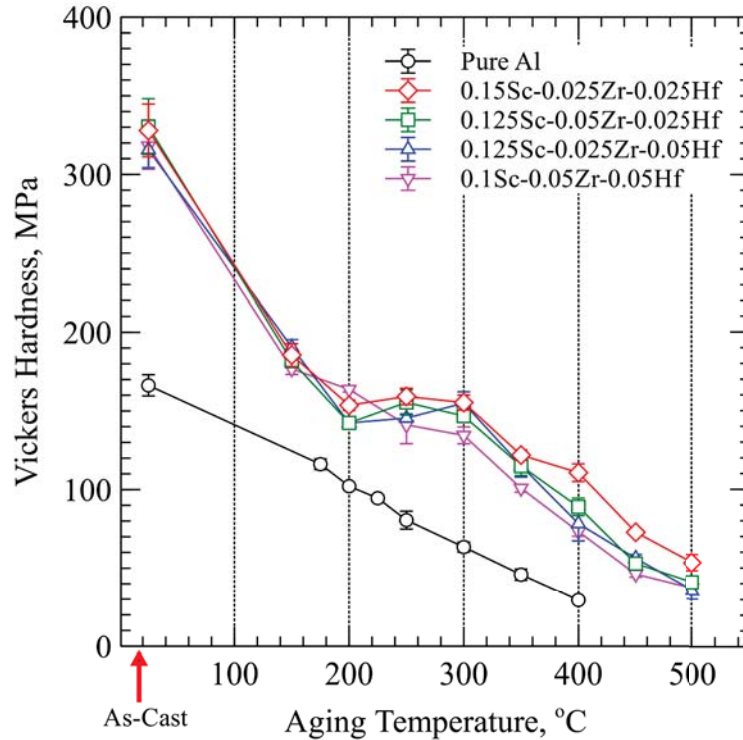


Fig. 4-7: Elevated-temperature macrohardness profile for a 3-hour multi-step, isochronal aging treatment up to 450°C. This is the same thermal treatment as in Fig. 4-5 except the hardness was measured at elevated temperatures.

The elevated-temperature hardness profiles of the peak-aged quaternary alloys (275°C-16 hours, 425°C-8 hours, 475°C-4 hours) are shown in Fig. 4-8, which also includes a comparison to A356 T-6, and a Ford piston under T-7 condition (Al-16Si-3Cu-1Mg, wt%). The quaternary alloys have initial room-temperature macrohardnesses greater than A356 T-6, but lower than the Ford piston alloy. However, the quaternary alloys all behave similarly to A356 above 150°C. The Ford piston alloy outperforms each alloy up to 500°C, at which point all the alloys converge. Additionally, overaging the quaternary alloys to produce over-ripened precipitates negatively effects both the room-temperature, and high-temperature hardness.

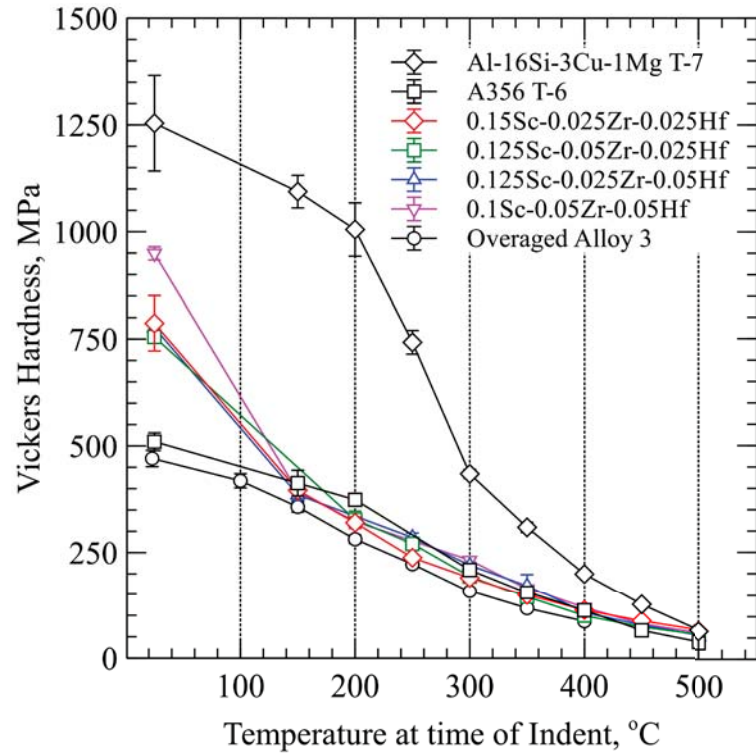


Fig. 4-8: Elevated-temperature macrohardness of various alloys

Room-temperature microhardness profiles of the binary alloys during the multi-step, isochronal heat-treatment are shown in Fig. 4-9. This shows a good correlation to the work done by Knipling, et al, for Al-Sc and Al-Zr (Fig. 1-4). The binary Al-Hf alloy shows a lesser hardening response, but at a similarly high temperature like Al-Zr.

ASTM grain measurements were calculated for Al-0.125Sc-0.025Zr-0.05Hf) and found to be -0.54 ± 0.033 . This would negate any Hall-Petch strengthening, as it does not have an effect on strengthening the material.

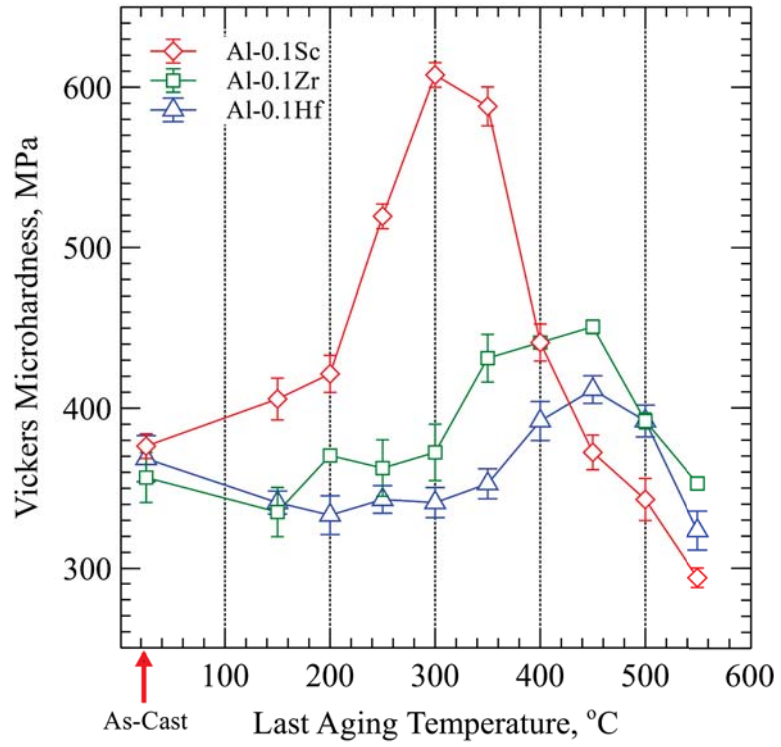


Fig. 4-9: Room-temperature microhardness profile of the Al-Sc, Al-Zr, and Al-Hf binary alloys during a 3hr multi-step, isochronal heat-treatment

4.3 Microstructure

Overaged samples were imaged by TEM to see precipitate morphology. Many of the precipitates have Ostwald ripened and are on the order of several tens of nanometers. Figure 4.7 is a bright-field image from the 0.125Sc-0.05Zr-0.025Hf, showing a ripened precipitate with a diameter ~ 20 nm. The upper left contains precipitates around 5 nm, which have not ripened. Qualitative EDS scans showed that the precipitates were rich in Sc, Zr, and Hf, while the matrix did show depletion of Sc, Zr, and Hf. However, the spot size could not be reduced for accurate observations of a “core-shell-shell” structure. No coherency observations were made.

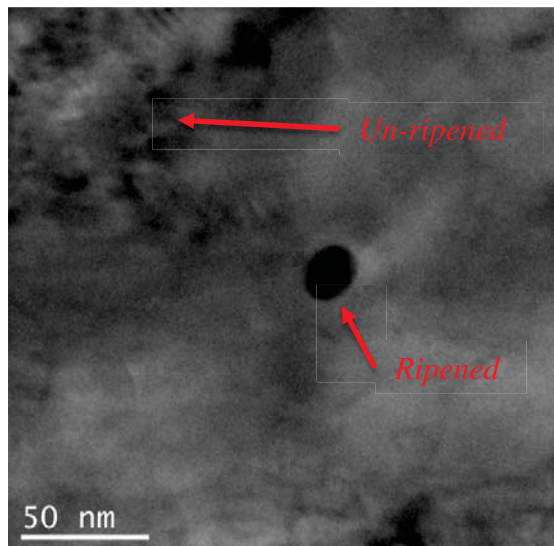


Fig. 4-10: Bright-field TEM image of 0.125Sc-0.05Zr-0.025Hf showing a ripened precipitated, depleted zone, and unripened precipitates.

In the EDS scans, the beam interacted with the Cu grid which resulted in the appearance of Cu peaks in the sample. This made distinguishing between Hf and Cu difficult. However, asymmetric peaks could be qualitatively differentiated to identify Hf. This can be seen in Fig. 4-11, an EDS scan from a precipitate, where the asymmetric, high-energy Cu peaks show broadening towards the Hf energy lines. Sc, Zr, and Hf levels were also higher in the precipitates than in the matrix (Fig. 4-12), indicating the depletion of matrix solute and enrichment as these solute atoms are incorporated in the precipitates.

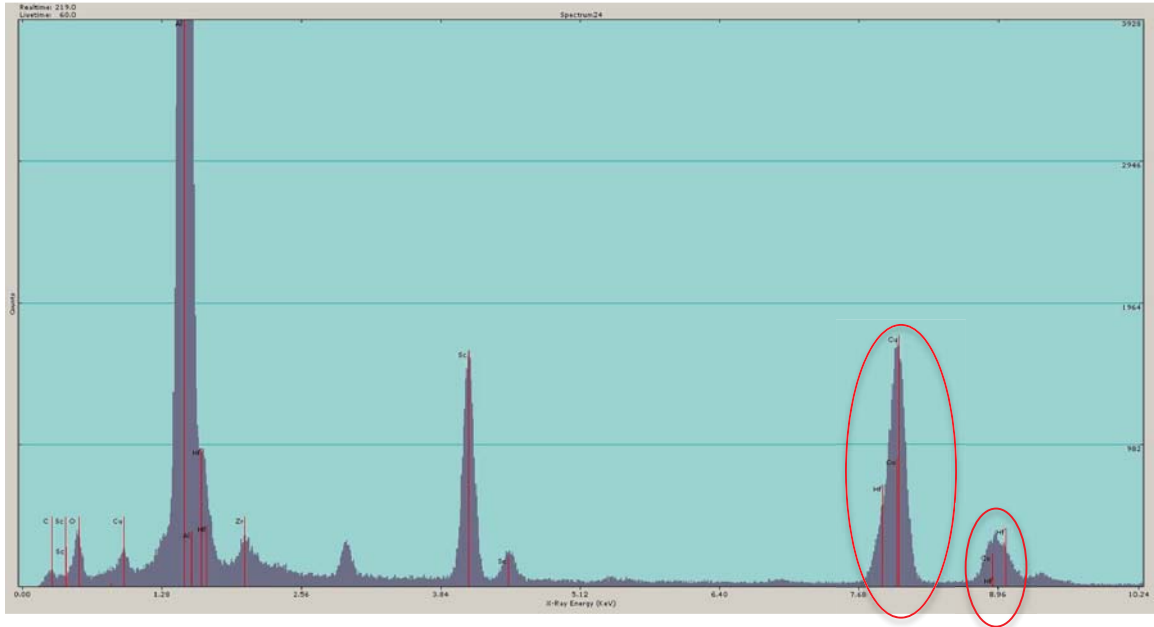


Fig. 4-12: EDS scan of a precipitate in Al-0.125Sc-0.05Zr-0.025Hf, showing Sc, Zr, and the shoulder of an Hf peak on the peak from the Cu grid.

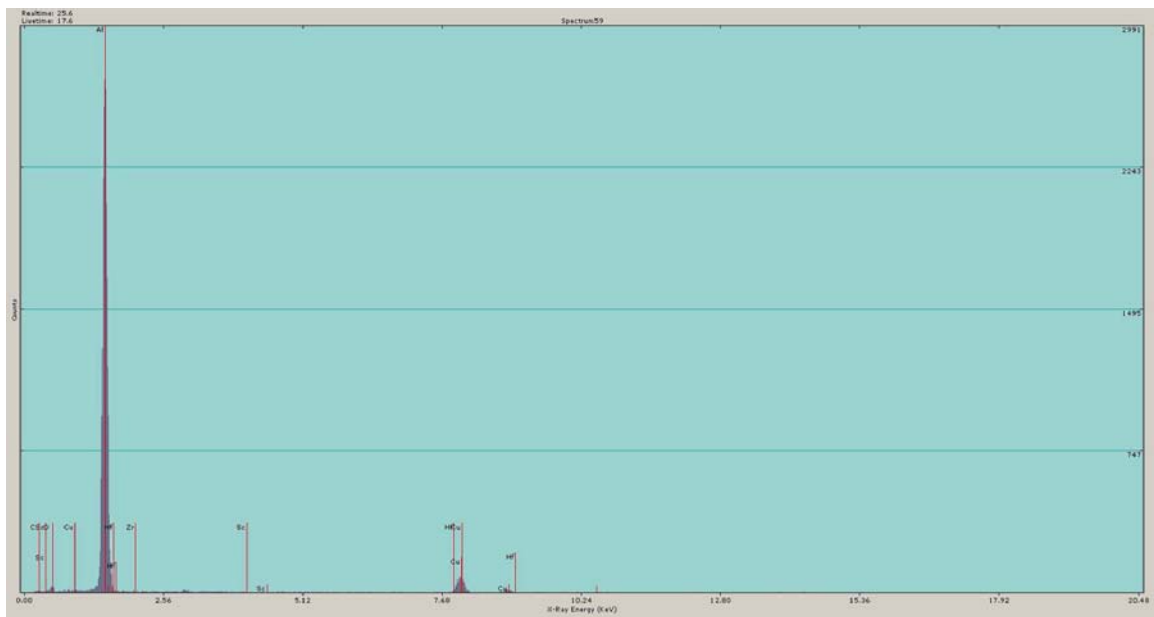


Fig. 4-11: EDS scan from the α -Al matrix in 0.125Sc-0.05Zr-0.025Hf.

5. Discussion

As determined using Thermo-Calc and Minitab to analyze the significance of the interactions between Sc, Zr, and Hf, four compositions of a quaternary alloy were isolated for mechanical characterization. Room-temperature hardness profile during the multi-step, isochronal aging treatment shows similarities to the studies performed by Knipling, et al.

Tables 5.1 show the diffusion lengths for the quaternary components, calculated from the data in Table 3.2. This is a relative calculation for the distance a solute atom can diffuse at a given temperature and length of time. An initial hardening response near 300°C corresponds to the precipitation of Al₃Sc particles, where the Sc atoms have enough mobility for precipitate formation. Zirconium and Hf, however have diffusion lengths on the order of atomic diameters at 300°C, indicating that they are not contributing to the initial onset of hardening. This can be calculated further for the case of the peak-aging alloys (Fig. 4-8) to estimate the distances during each aging step, shown in Table 5-2. The italicized values show the distances that were targeted for each specific step.

Table 5-1: Diffusion Lengths in Aluminum after 3 hours

	Diffusion Length (nm)		
	200°C	300°C	400°C
Sc	1.34	62.4	926
Zr	0.00244	0.523	22.8
Hf	0.00106	0.223	9.55

Table 5-2: Diffusion Lengths Through Aluminum After Each Heat Treatment Step

	Diffusion Length, nm		
	275°C	425°C	475°C
	16 hours	8 hours	4 hours
Sc	62.92	2631.16	5038.81
Zr	0.38	<i>80.70</i>	229.96
Hf	0.16	33.72	<i>95.54</i>

The hardness profiles from Fig. 4-5 also indicated a secondary hardening response at 450°C in the 0.15Sc-0.05Zr-0.025Hf and 0.1Sc-0.05Zr-0.05Hf samples. Though above the reported hardness values from Knipling, et al, the longer diffusion lengths of Zr and Hf would lead to the additional precipitation of Al₃Zr or Al₃Hf. The 0.125Sc-0.05Zr-0.025Hf also showed the highest hardness at 500°C, ~620 MPa, which was 50-100 MPa higher than the other three in Fig. 4-5.

Elevated-temperature hardness and conductivity profiles show a similar response at 250°C. The increase in conductivity at 250°C for the alloy with 0.15 at% Sc suggests that Al₃Sc precipitates begin to nucleate, lowering the amount of Sc atoms in the supersaturated α -Al matrix. This is also confirmed with the elevated-temperature hardness, where, between 200-300°C, the hardness remains the same, or increases, though a decrease in hardness was observed for pure aluminum. After the initial diffusion of Sc to producing Al₃Sc, linear decrease in hardness from 300-450°C suggests that there is little strengthening effect from further precipitation hardening due to the group IV elements Zr and Hf. However, Al-0.15Sc-0.025Zr-0.025Hf alloy did show a non-linear decrease from 300-450°C, with a slight improvement in a loss of hardness at 400°C. At 450°C, the peak conductivity was reached by all four compositions, where there was a significant drop in hardness down to 35-55 MPa.

The lack of secondary response could be attributed to the lack of Zr or Hf that is supersaturated in the Al matrix. The 0.1Sc-0.05Zr-0.05Hf sample showed a significantly higher conductivity in the as-cast state, a sign of fewer Sc, Zr, or Hf atoms in solution. It may be possible that the Hf decreases the overall solute solubility in Al, causing less Sc and Zr to dissolve into the matrix. This is not advantageous, as it decreases the possible precipitation volume fraction during aging. The samples with 0.05 at% Hf also showed a lower maximum conductivity of $33.2 \pm 0.1 \text{ MS}\cdot\text{m}^{-1}$, where the samples with 0.025 at% Hf peaked at $34.3 \pm 0.1 \text{ MS}\cdot\text{m}^{-1}$. The higher values of conductivity indicates that more solute atoms have diffused out of the matrix into precipitate form. Lower conductivity indicates

the alloy has fewer precipitates, which is not advantageous as it generally indicates lower Orowan strengthening.

The peak-aged quaternary alloys (Table 4-1) show high-temperature hardness behavior similar to A356, while having room-temperature hardness between A356 and the Ford piston. The large drop in hardness at 150°C of the peak-aged quaternary alloys indicates that there is a mechanism for deformation that is not effected by Orowan strengthening in these alloys.

TEM micrographs of the overaged samples revealed large precipitates that were not homogenously dispersed. These had begun to undergo Ostwald ripening, and reduced the number density of the precipitates. There were clusters of unripened precipitates were present, however. The larger precipitates were on the order of 20-50 nm in diameter, while smaller precipitates were ~5 nm.

While only qualitative EDS analysis was performed, the depletion of Sc, Zr, and Hf in the matrix does show that the solute were able to remain out of solution up to 450°C. This was also confirmed by the peak conductivity of all four compositions. The additions of Zr and Hf, though not adding a secondary response in hardness, may be enhancing the stability of Al₃Sc precipitates by reducing the volume-diffusion of Sc through the α -Al matrix.

The coarse-grained structure of these alloys indicates that the increased room-temperature hardness increase was not associated with reduced grain size strengthening as in the Hall-Petch relationship. This would also indicate that the decrease in hardness above room-temperature is attributed to a thermally-activated deformation mechanism that bypasses the precipitate structure.

6. Future Work

This work focused only on a multi-step isochronal heat treatment. Further studies to collect data for isothermal heat treatments are needed, and eventually an optimized heat treatment will be required as well. More iterations of the three step aging treatment would be necessary to provide Sc, Zr, and Hf proper time to diffuse at specific to their specific core-shell-shell configuration.

Additionally, hardness was the only mechanical characterization method performed. For more detailed analysis, tensile data should be collected (especially at elevated temperatures), as well fatigue and creep testing.

More microstructural analysis is needed during each aging step. Detailed microstructure changes from nucleation, to growth and overaging, as well as the coherency of the precipitates should be studied. Higher resolution techniques are needed for further investigation on the ability to form “core-shell-shell” precipitate structures.

Most importantly, however, would be for future work to be focused on the mechanism these alloys have for high-temperature strengthening. Previous studies agree that the nano- Al_3X show promise for high-strength, low-alloy alloy designs, but this work shows that they do not have outstanding high-temperature strength. Understanding the fundamental atomistic behavior will undoubtedly provide insight into producing alloys of this nature to experience enhanced high-temperature strength.

7. Conclusions

Through detailed designed experiments and thermodynamic modelling, Hf was selected to be analyzed as a quaternary alloying addition to the Al-Sc-Zr ternary system, as it showed a response of an increase to the total precipitate fraction from 600-400°C.

Adding small amounts of Hf to low-alloy Al-Sc-Zr provided a secondary hardening response at 450°C during a multi-step, isochronal aging treatment when test at room-temperature.

Elevated-temperature hardness profiles during a multi-step, isochronal aging treatment showed an increase in hardness from 200-300°C, due to the precipitation of Al₃Sc, which was confirmed by an increase in conductivity. However, no secondary hardness response from Zr or Hf was seen above 300°C, even as conductivity continues to increase.

High-temperature hardness of the peak-aged samples showed behavior similar to A356. However, a large drop in hardness at 150°C shows that there must be a mechanism for deformation that is bypassing the nano-precipitate structure, as the coarse grain size would negate any strengthening due to the Hall-Petch relationship.

TEM images taken up to the 450°C aging step revealed precipitates that had begun to undergo Ostwald ripening. However, the EDS analysis was inconclusive for the determination of a “core-shell-shell” precipitate structure. However, EDS analysis did reveal lower Sc, Zr, and Hf in the matrix as compared to the precipitate, indicating that they remained out of solution up to 450°C.

References

- [1] Hosford WF. Mechanical Behavior of Materials 2nd Edition. New York, NY; Cambridge University Press; 2010.
- [2] Knipling KE, Dunand DC, Seidman, DN. Criteria for developing castable, creep-resistant aluminum-based alloys – A review. *Zeitschrift fur Metallkunde*. 2006; 97 (3): 246-265
- [3] L.A. Willey U.S. Patent 3,619,181 (1971)
- [4] Totten GE, MacKenzie DS. Handbook of Aluminum Vol. 1: Physical Metallurgy and Processes. New York, NY; Marcel Dekker; 2003.
- [5] Toropova LS, Eskin DG, Kharakterova ML, Dobatkina TV. Advanced Aluminum Alloys Containing Scandium. 1st Milton Park, Abindon, Oxon: Taylor & Francis; 1998.
- [6] Murray JL. Al-Sc Phase Diagram, ASM Alloy Phase Diagrams Center, P. Villars, editor-in-chief; H. Okamoto and K. Cenzual, section editors; <http://www1.asminternational.org/AsmEnterprise/APD>, ASM International, Materials Park, OH; 2006.
- [7] Knipling KE, Seidman DN, Dunand DC. Ambient- and high-temperature mechanical properties of isochronally aged Al-0.06Sc, Al-0.06Zr and Al-0.06Sc-0.06Zr (at%) alloys. *Acta Materialia*. 2011; 59: 943-954
- [8] Knipling KE, Karnesky RA, Lee CP, Dunand DC, Seidman DN. Precipitation evolution in Al-0.1Sc, Al-0.1Zr and Al-0.1Sc-0.1Zr (at%) alloys during isochronal aging. *Acta Materialia*. 2010; 58: 5184-5195.

- [9] Fuller CB, Seidman DN, Dunand DC. Mechanical properties of Al(Sc,Zr) alloys at ambient and elevated temperatures. *Acta Materialia*. 2003; 59: 4803-4814.
- [10] Okamoto H. Al-Zr Phase Diagram, ASM Alloy Phase Diagrams Center, P. Villars, editor-in-chief; H. Okamoto and K. Cenzual, section editors; <http://www1.asminternational.org/AsmEnterprise/APD>, ASM International, Materials Park, OH; 2006.
- [11] Knipling, KE, personal communication
- [12] van Dalen ME, Dunand DC, Seidman DN. Precipitation strengthening in Al(Sc,Ti) alloys. *Materials Science and Technology, Affordable Metal Matrix Composites for High Performance Applications II*. 2003; 195-201.
- [13] Hallem H, Fordbord B, Marthinsen K. An investigation of cast structures in Al-Hf-(Sc)-(Zr) alloys and their subsequent effect on recrystallisation resistance after cold rolling. *Materials Australia*. 2004; 28: 240-245.

A. Appendix



COPYRIGHT PERMISSION REQUEST

Please complete all contact information:

Name: Matthew Wong Title: Graduate Research Assistant
Company/Organization: Michigan Technological University
Address: 1400 Townsend Dr, M&M Building Rm 512
City/State/Zip/Country: Houghton, MI 49931, USA
Phone: 651-231-9046 Email: mjwong@mtu.edu

I am preparing an article/chapter for publication in the following formats (check as applicable):
Print Only Internet Only Print and Electronic Media

The information will be used for (check as applicable):
Journal article Conference presentation Internal company records
Dissertation Student course material Commercial publication*

Please complete the following:

The article/chapter title will be: Introduction
The publication title will be: DEVELOPMENT OF PRECIPITATION HARDENABLE AL-SC-ZR-HF QUATERNARY ALLOYS THROU
Publisher: Michigan Technological University
Planned date of publication: Sp/Summer 2014

I hereby request permission for non-exclusive world rights for the above publication and all subsequent editions, revisions, and derivative works in English and foreign translations, in the formats indicated above from the following copyrighted content by ASM International:

Book ISBN: Copyright date: 1998
Book/Publication title: J. Phase Equilibrium
Author name(s): Murray, J.L.
Article title: The Al-Sc (Aluminum-Scandium) System
Text page numbers:
Figure numbers (with page numbers):
Table numbers (with page numbers):

Signature: 

Date: 4-21-2014

FOR ASM INTERNATIONAL USE ONLY:

I (we) grant permission requested above. Please ensure that ASM International receives proper credit as publisher by citing the above ASM publication as a reference and including the following: Reprinted with permission of ASM International. All rights reserved. www.asminternational.org

ASM International Representative: 

Date: 4-24-2014

*For Commercial Publications, a copyright permission fee of \$50 per figure will be assessed. Exceptions can be made for reuse of content by its original authors.

ASM International, Permissions, 9639 Kinsman Road, Materials Park, Ohio 44073-0002
permissions@asminternational.org, Phone: 440-338-5151 x5465, Fax: 440-338-8542

SUBMIT

Fig. A-1: Right to publish material from ASM for the Al-Sc Phase diagram from Fig. 1.2.



COPYRIGHT PERMISSION REQUEST

Please complete all contact information:

Name: Matthew Wong Title: Graduate Research Assistant
Company/Organization: Michigan Technological University
Address: 1400 Townsend Dr, M&M Building Rm 512
City/State/Zip/Country: Houghton, MI 49931, USA
Phone: 851-231-9046 Email: mjwong@mtu.edu

I am preparing an article/chapter for publication in the following formats (check as applicable):
Print Only [] Internet Only [] Print and Electronic Media [x]

The information will be used for (check as applicable):
Journal article [] Conference presentation [] Internal company records []
Dissertation [x] Student course material [] Commercial publication* []

Please complete the following:
The article/chapter title will be: Introduction
The publication title will be: DEVELOPMENT OF PRECIPITATION HARDENABLE AL-SC-ZR-HF QUATERNARY ALLOYS THROL
Publisher: Michigan Technological University
Planned date of publication: Sp/Summer 2014

I hereby request permission for non-exclusive world rights for the above publication and all subsequent editions, revisions, and derivative works in English and foreign translations, in the formats indicated above from the following copyrighted content by ASM International:

Book ISBN: Copyright date: 2002
Book/Publication title: J. Phase Equilibrium
Author name(s): Okamoto, H
Article title: Al-Zr (Aluminum-Zirconium)
Text page numbers:
Figure numbers (with page numbers):
Table numbers (with page numbers):

Signature: [Redacted] Date: 4-21-2014

FOR ASM INTERNATIONAL USE ONLY:
I (we) grant permission requested above. Please ensure that ASM International receives proper credit as publisher by citing the above ASM publication as a reference and including the following: Reprinted with permission of ASM International. All rights reserved. www.asminternational.org

ASM International Representative: [Redacted] Date: 4-24-2014

*For Commercial Publications, a copyright permission fee of \$50 per figure will be assessed.
Exceptions can be made for reuse of content by its original authors.

ASM International, Permissions, 9639 Kinsman Road, Materials Park, Ohio 44073-0002
permissions@asminternational.org, Phone: 440-338-5151 x5465, Fax: 440-338-8542

SUBMIT

Fig. A-2: Right to publish material from ASM for the Al-Zr Phase diagram from Fig. 1.3.